Support Information

Accelerating the Design of Multi-component Nanocomposite Imprinted Membrane by Integrating a Versatile Metal-Organic Methodology with Mussel-Inspired Secondary Reaction Platform

Yilin Wu[a], Ming Yan[b], Xinlin Liu[c], Peng Lv[b], Jiuyun Cui[a], Minjia Meng[a], Jiangdong Dai[b], Yongsheng Yan[a], Chunxiang Li[a,]*

[a] *School of Chemistry and Chemical Engineering, Jiangsu University, Zhenjiang 212013, China*

[b] *School of Material Science and Engineering, Jiangsu University, Zhenjiang 212013, China*

[c] *School of Energy and Power Engineering, Jiangsu University, Zhenjiang 212013, China*

Experimental Details

The ATR-FTIR spectra (4000-500 cm^{-1}) for modified ACMs were recorded on a FT-IR Nicolet560 apparatus (Nicol, U.S.A.), and ZnSe was used as the crystal plate. A contact angle measuring system (G10 Kruss, Germany) was used to measure the static water contact angle of membranes. The deionized water droplet was placed on a dry flat membrane surface and the contact angle was obtained. The reported contact angle value was calculated by averaging over more than five contact angle values at different sites for insuring the accuracy.

Detailed test conditions of HPLC

The solvent of samples was volatilized under vacuum and then methanol (HPLC grade) was applied to dissolve the dry samples. The conditions of determination were as follows: methanol/H_2O (70/30, v/v) mobile phase, 1.0 mL min^{-1} flow rate, 280 nm UV detection and 25 ^oC column temperature.

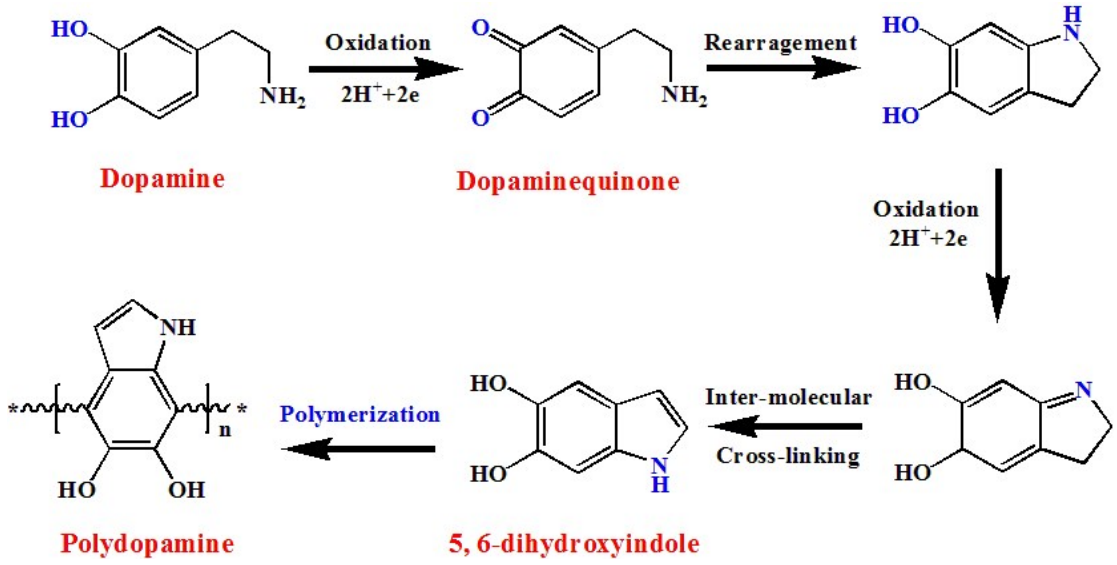

Figure S1 Possible reaction mechanism for dopamine polymerization.

Dopamine could polymerize and stick on all kinds of organic and inorganic surfaces through the formation of strong covalent and noncovalent bonds with surfaces. The polymerization mechanism of dopamine was proposed as interaction of a noncovalent self-assembly and a covalent polymerization through oxidation of catechol to dopaminequinone under an aerobic and alkaline condition and then further oxidizes and polymerizes through deprotonation and intermolecular Michael addition reaction to form a cross-linked homopolymer. The functional groups such as catechol, amine, and imine can serve as both the starting points for covalent modification with desired molecules and the anchors for the loading of transition metal ions, which can further realize the emergence of diverse hybrid materials by virtue of its powerful reducing capability toward these metal ions under basic conditions.

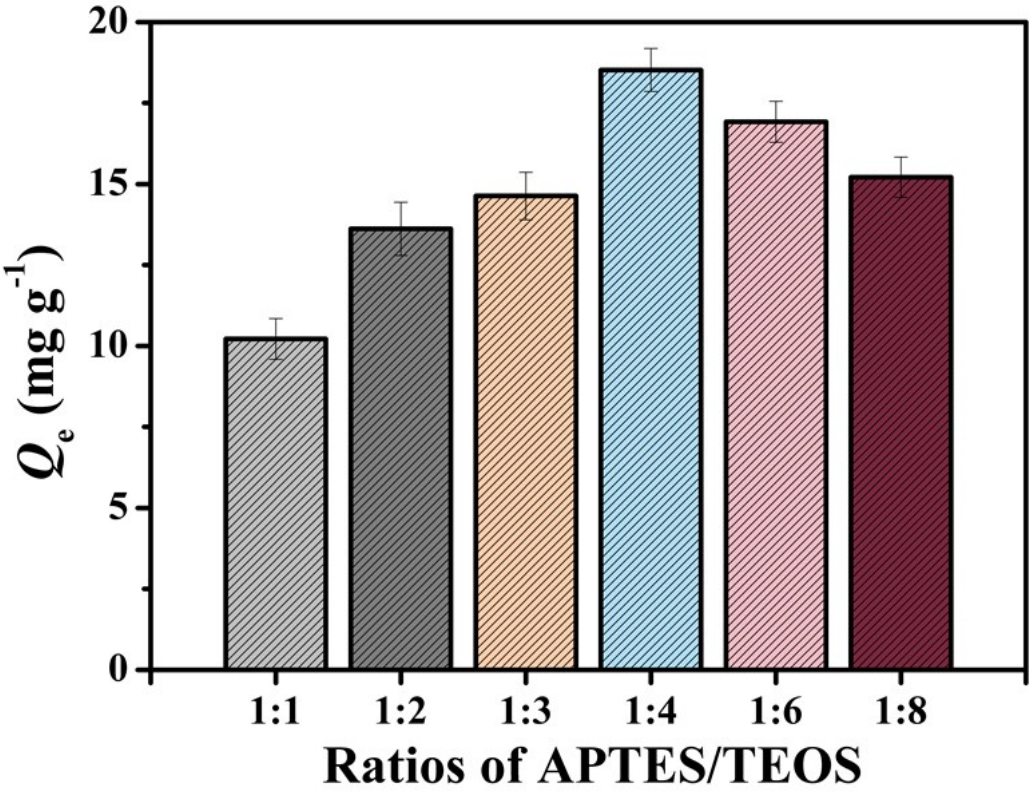

Figure S2. The influence of the ratio of APTES/TEOS on the adsorption capacity of MMO-MIM

In order to reduce error and increase measurement precision, the fixed factors like adsorption concentration of m-cresol (600 mg L^{-1}) and adsorption temperature (25 ^{o}C) were used as the constant adsorption conditions in the whole optimized experiments. During the MMO-MIM synthesis, 0.5 mmol m-cresol and different ratios of APTES/TEOS (0.2:0.2, 0.2:0.4, 0.2:0.6, 0.2:0.8, 0.2:1.2, and 0.2:1.6 mL/mL) were chosen to study. As shown in Figure S2, when the ratio of APTES/TEOS is 1:4 (0.2:0.8 mL/mL), the maximum adsorption amount (18.55 mg g^{-1}) is obtained.

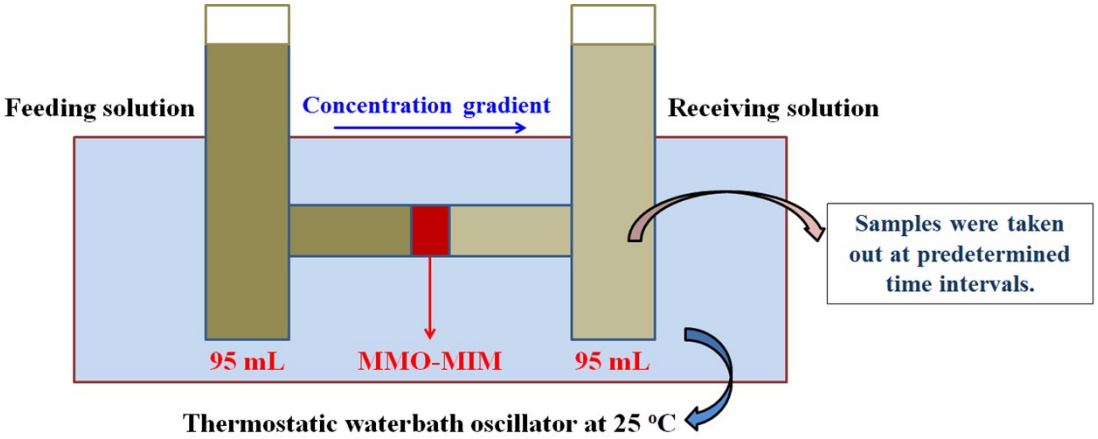

Figure S3 The thermostatic waterbath permeation installation of permeation experiments.

As depicted in Figure S2, the selectivity permeation character of MMO-MIM was evaluated toward competitive substrates m-cresol and 2,4-DP. The isomer permeation experiments were carried out at room temperature using different concentrations of m-cresol (100, 200, 400, 600, 800, 1000 mg L^{-1}) as the feeding solution.

The time-dependent selective permeation experiments toward m-cresol and 2,4-DP were carried at 25 °C with the concentration of 400 mg L^{-1}. The membrane, with an effective area of 1.5 cm^2, was fixed solidly between two chambers of a permeation cell. The volume of each chamber was 150 mL. The mixture solution of m-cresol and 2,4-DP in ethanol (95 mL) was placed in the left-hand side chamber, while 95 mL ethanol was placed in the right-hand side chamber.

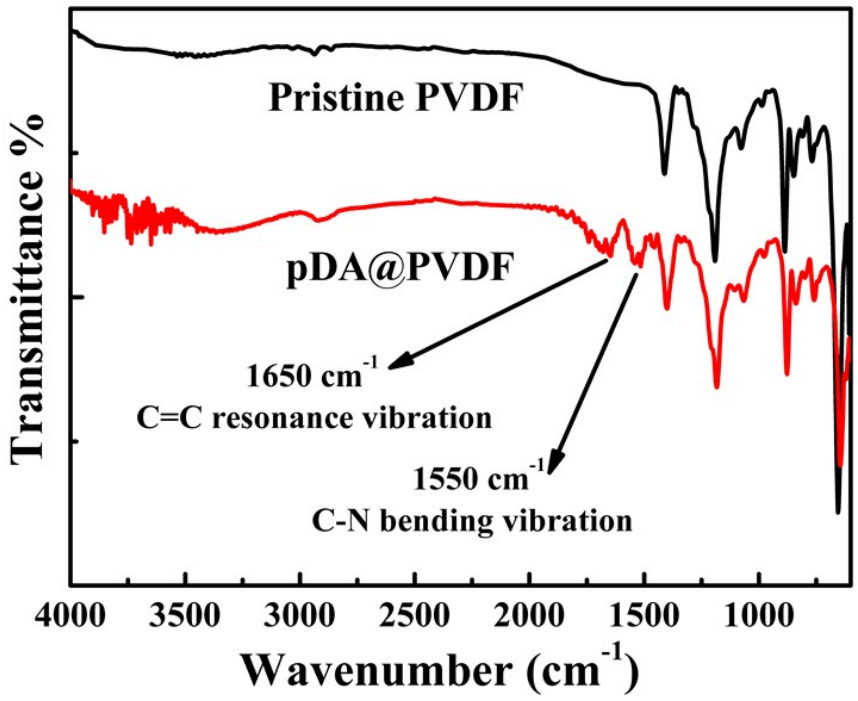

Figure S4. ATR-FTIR spectra of pristine PVDF and pDA@PVDF.

The ATR-FTIR spectra of pristine PVDF and pDA@PVDF are further investigated to analyze the pDA modification procedure on PVDF. As shown in the ATR-FTIR spectra in Figure S4, compared with ATR-FTIR data with pristine PVDF, the pDA@PVDF displayed several new absorption signals at 1550 cm^{-1} and 1650 cm^{-1}, suggesting the occurrence of N-H bending vibrations and C=C resonance vibrations C=C resonance vibrations in the aromatic ring, respectively. In addition, a broad absorbance between 3700 and 3000 cm^{-1} is ascribed to O-H and NH_2 stretching vibrations. This observation evidently suggested the successful formation of pDA polymer layers on the surface of pristine PVDF.

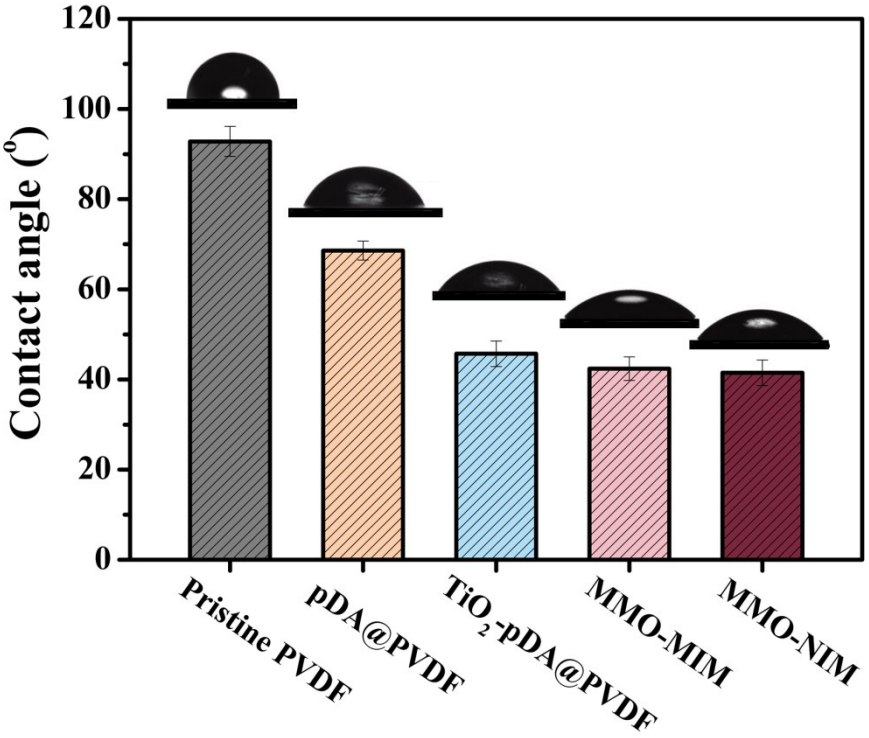

Figure S5. Water contact angle of various membranes

Water contacting angle measurement was also done to further verify the surface hydrophilicity of various membranes. In general, the smaller contact angle indicates the better hydrophilicity of membranes. The contact angle results of membranes are shown in below or in Figure S5 in Supporting Information. The water contact angle of pristine PVDF membrane decreases from 92.8° to 68.6° after being modified by pDA for 6h, and the value of water contact angle (68.6°) of pDA@PVDF is similar to the data reported in other literature.[3-4] This phenomenon also demonstrates that the pDA-based layers containing hydrophilic groups have been successfully introduced onto the pristine PVDF. After the TiO_2 modification, water contact angles decrease significantly from 68.6° to 45.7°, implying the impressive enhancement in hydrophilicity. After the sol-gel imprinting procedure, water contact angle of MMO-MIM decreases little from 45.7° to 42.4°, and the MMO-NIM keep nearly a similar same water contact angle at 41.5°, which suggested the as-prepared MMO-MIM processed excellent hydrophilicity after the imprinting procedure.

Discussion Details

Langmuir analysis

To further study the isomer adsorption properties of MMO-MIM, Langmuir isotherm adsorption model was used for fitting the experimental data to investigate the adsorption mechanism in detail. Langmuir isotherm adsorption model was used for fitting the experimental data to understand the adsorption mechanism of MMO-MIM and MMO-NIM.[5] The Langmuir equation is listed as follow:

$$Q_e = \frac{K_L Q_m C_e}{1 + K_L C_e} \quad (1)$$

where Q_e (mg g^{-1}) and Q_m (mg g^{-1}) represent the equilibrium and maximum adsorption capacity of template molecules, respectively. C_e (mg L^{-1}) is the equilibrium concentration of template molecule, K_L (L mg^{-1}) is the Langmuir constant. The linear regression values fitting with Langmuir model and the data of isothermal adsorption experiments are listed in Table S1. As shown in Figure 6 and Table S1, it could be seen that the Langmuir isotherm model fitted well with experimental data, indicating the excellent imprinting factor of MMO-MIM. In addition, the linear Langmuir plot and the appropriate fitting curve (K_L, 0.0046 L mg^{-1}; R^2, 0.9972) might also originate from the homogeneous distribution of imprinting layers on the surface of MMO-MIM.

Table S1. Langmuir data for the adsorption of m-cresol onto MMO-MIM and MMO-NIM at 25 °C.

Membranes	$Q_{e,exp}$ (mg g^{-1})	$Q_{e,c}$ (mg g^{-1})	K_L (L mg^{-1})	R^2
MMO-MIM	19.17	19.30	0.0046	0.9972
MMO-NIM	6.463	6.459	0.0045	0.9967

Kinetics analysis

The pseudo-first-order[4] and pseudo-second-order[5] rate equations were applied to further invsetigate the kinetic properties of MMO-MIM. The pseudo-first-order (2) and pseudo-two-order (3) equations are listed as follows:[6-7]

$$Q_t = Q_e - Q_e e^{-k_1 t} \quad (2)$$

$$Q_t = \frac{k_2 Q_e^2 t}{1 + k_2 Q_t t} \quad (3)$$

where Q_e (mg g^{-1}) and Q_t (mg g^{-1}) are the adsorption amounts of MMO-MIM and MMO-NIM at equilibrium with different contact time t. k_1 (min^{-1}) and k_2 (g mg^{-1} min^{-1}) are constants of first-order model and second-order model, respectively.

The pseudo-two-order fitting curves and binding data from kinetic adsorption experiments of MMO-MIM and MMO-NIM are described in Figure 6. And the results such as linear regression values and adsorption rate constants from two models are listed in Table S2. R^2 values calculated from second-order model (0.9953) were found to be significantly higher than that of the first-order model, the Q_e values calculated from second-order model were simultaneously close to the experimental data. As described in the end, the results from pseudo-two-order model fitted better than that of pseudo-second-order model, suggesting the significant influence of chemical reactions in the adsorption process and the specific recognition forces between MMO-MIM and template molecules.

Table S2. Kinetics constants for the pseudo-first-order and pseudo-second-order rate equations.

Membranes		Pseudo-first-order model			Pseudo-second-order model		
	$Q_{e,exp}$ (mg g^{-1})	$Q_{e,cal}$ (mg g^{-1})	k_1 (min^{-1})	R^2	$Q_{e,cal}$ (mg g^{-1})	k_2 (g mg^{-1} min^{-1})	R^2
MMO-MIM	19.11	24.38	0.0144	0.8704	19.34	0.0033	0.9979

MMO-NIM	6.682	10.02	0.0111	0.8844	6.742	0.0079	0.9977

Adsorption regeneration experiments

To investigate the regeneration and stability character of MMO-MIM, the regenerate adsorption experiments were performed at the concentration of 600 mg L^{-1} for three times by the same adsorbed membrane at 25 ^{o}C. After adsorption, the saturated adsorbed TMICMs were eluted with the mixture of methanol and acetic acid (95:5, v/v) by Soxhlet extraction to remove the template molecules. And then the regenerated MMO-MIM was used for subsequent adsorption cycles (adsorption/desorption).

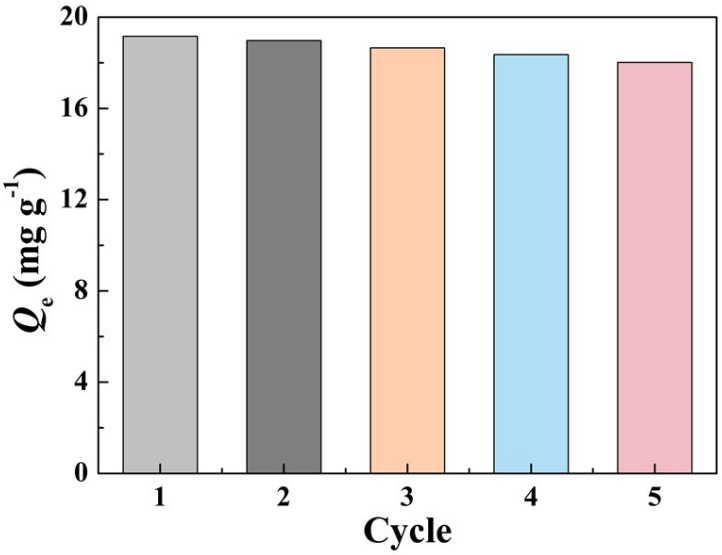

Figure S6. Adsorption stability and regeneration performances of MMO-MIM after several adsorption-desorption cycles.

References:

[1] Q. Liu, N. Y. Wang, J. Caro, A. S. Huang, *J. Am. Chem. Soc.*, 2013, **135**, 17679.

[2] H. Lee, S. M. Dellatore, W. M. Miller, P. B. Messersmith, *Science*, 2007, **318**, 426.

[3] J. H. Li, Y. Y. Xu, L. P. Zhu, J. H. Wang, C. H. Du, *J. Membr. Sci.*, 2009, **326**, 659.

[4] P. Zhang, C. Shao, Z. Zhang, M. Zhang, J. Mu, Z. Guo, Y. Liu, *Nanoscale*, 2011, **3**, 2943.

[5] I. Langmuir, *J. Am. Chem. Soc.*, 1918, **40**, 1361.

[6] Y. S. Ho, G. McKay, *WaterRes.*, 1999, **33**, 578.

[7] Y. S. Ho, G. McKay, *Process Biochem.*, 1999, **34**, 451.